Brillouin integrated photonics

Benjamin J. Eggleton[1], Christopher G. Poulton[2], Peter T. Rakich[3], Michael. J. Steel[4], Gaurav Bahl[5]

[1] *University of Sydney Nano Institute (Sydney Nano), Institute of Photonics and Optical Science (IPOS), School of Physics, University of Sydney, NSW 2006 Australia*

[2] *School of Mathematical and Physical Sciences, University of Technology Sydney, NSW 2007, Australia*

[3] *Department of Applied Physics, Yale University, New Haven, CT 06520 USA*

[4] *MQ Photonics Research Centre and Department of Physics and Astronomy, Macquarie University, New South Wales 2109, Australia*

[5] *Mechanical Science and Engineering, University of Illinois Urbana Champaign, 1206 W. Green St., Urbana, IL 61801, USA*

Abstract

A recent renaissance in Brillouin scattering research has been driven by the increasing maturity of photonic integration platforms and nanophotonics. The result is a new breed of chip-based devices that exploit acousto-optic interactions to create lasers, amplifiers, filters, delay lines and isolators. Here we provide a detailed overview of Brillouin scattering in integrated waveguides and resonators, covering key concepts such as the stimulation of the Brillouin process, in which the optical field itself induces acoustic vibrations, the importance of acoustic confinement, methods for calculating and measuring Brillouin gain, and the diversity of materials platforms and geometries. Our review emphasizes emerging applications in microwave photonics, signal processing and sensing, and concludes with a perspective for future directions.

1. Introduction

Stimulated Brillouin scattering, a process that results from a form of coherent light-sound coupling[1–3], has a rich history in the realm of laser physics[4] and nonlinear optics[3,5–13]. Brillouin interactions give rise to a third order optical nonlinearity, with a strength that often exceeds Kerr and Raman interactions by orders of magnitude[4,14]. Brillouin scattering also has several distinct and useful properties that arise directly from the fact that the interaction arises from coupling between optical fields and phonons in the GHz frequency range. Within solid and fluid bulk media, this interaction has been used to realize new laser sources, determine elastic properties, and perform phase conjugation and precision spectroscopy, in addition to a range of useful tasks and applications. Moreover, the same underlying mechanism for the light-sound coupling that produces the Brillouin effect also gives rise to linear acousto-optic interactions, which are the basis for modern acousto-optic signal processing technologies [15]. Over the past decade there have been remarkable developments in the control of *integrated* Brillouin interactions and in the novel waveguides and platforms that have been used to harness them. Brillouin scattering was for many years confined to experiments in tens of metres of optical fibre[16–18], in which the gain spectrum was fixed and where Brillouin properties were almost identical to those of bulk materials. This situation began to change in 2006, when it was shown that microstructured optical fibres (in this case, fibres with core diameters of order 1 μm suspended by threads of order 100 nm across,) could be used to control the shape of the SBS spectrum[19]. This was soon followed by the demonstration that Brillouin gain could also be enhanced in a photonic crystal fibre[20], due to the tight confinement of both optical and acoustic fields in the microstructured core. These demonstrations, together with new theoretical work[21] that suggested that Brillouin interactions could be greatly magnified by radiation pressure on micron-scale waveguide boundaries, highlighted the possibility of harnessing SBS over centimetre-scale propagation lengths. This triggered a period of intense research interest into materials and waveguide geometries that would enable Brillouin scattering to be harnessed in chip-scale environments.

A central problem to be solved in integrated Brillouin applications is the simultaneous confinement of the optical and acoustic waves[22,23]. For example, while silicon-on-insulator (or silicon nanowire) waveguides confine light through total internal reflection (TIR), the high stiffness of the silicon waveguide core prevents a corresponding form of elastic wave guidance. A first solution to the confinement problem, and the first demonstration of SBS in an integrated photonic environment, was found in the chalcogenide soft glass platform,[24] where the high refractive index and relatively low stiffness of As_2S_3 glass allowed for confinement of both optical and elastic waves by TIR. An alternate approach to acoustic confinement is to mechanically isolate the optically guiding core from the substrate: the first demonstrations of this kind used suspended silicon waveguides[25] and micron-scale waveguides with tapered supports[26]. A third strategy is simply to manage without acoustic confinement, an approach that has been demonstrated using ultra-low loss waveguide systems wherein the relatively low gain produced by the waveguide is compensated by resonant enhancement

of the Brillouin interaction within an optical cavity[27–33]. In spite of these successes, the search for easily-manufactured, mechanically-robust waveguide systems that can jointly confine light and high-frequency (~GHz) sound in silicon or other popular semiconductor platforms remains a key challenge. Regardless of the approach, the ability to induce, enhance, and harness SBS interactions provides new opportunities to utilize Brillouin interactions on a chip in ways that greatly extend how Brillouin effects have traditionally been exploited in optical fibre and bulk systems, as we detail below. With such rapid development it is difficult to predict all the opportunities that these complementary systems and strategies may provide, and thus where this field might be heading.

In this paper, we explore the diverse array of strategies that have been used to enhance and shape Brillouin interactions within integrated photonic waveguide systems, as well as some of the goals and motivations of the growing field of integrated Brillouin photonics. Our main focus is on quasi-planar waveguide geometries, but we also address planar-compatible structures such as toroidal and spherical microresonators. Within the growing ecosystem of integrated Brillouin photonics, all these systems offer unique opportunities for applications that range across modern communications, radar, sensing and navigation. Throughout the paper, we discuss these developments in integrated Brillouin photonics with the understanding that these results build upon prior foundational studies in the context of nonlinear optics and fibre optics.

2. Elements of Brillouin scattering and material requirements

Brillouin scattering arises from the interaction of light with phonons – acoustic waves – that exist within a transparent material or waveguide (Fig 1). These acoustic waves may be driven externally, excited optically, or be associated with intrinsic thermal phonons. Whichever of several Brillouin scattering interactions is used (see Box 1), the underlying principle remains the same: phonons perturb the local material properties both by deforming the physical boundaries of the material and by changing the permittivity of the waveguide through photoelasticity (though the relative importance of these two contributions varies greatly depending on the waveguide size and shape). This perturbation scatters light from an incident optical pump to a Stokes signal (or anti-Stokes) that is downshifted (upshifted) from the pump by the phonon frequency. Simultaneously, interference of the incident and scattered optical fields produces forces that create or annihilate phonons. This process can form a feedback loop – *stimulated* Brillouin scattering, or SBS – through which the Stokes field is exponentially amplified. The distinctive feature of SBS, and indeed of all Brillouin interactions, is the creation of an extremely narrow Stokes line that is typically downshifted in frequency from the pump by an amount in the MHz-GHz range (Fig. 1). These frequencies are the direct result of the acoustic nature of the interaction, with the Brillouin shift equal to the phonon frequency and the linewidth of the Brillouin gain arising from the phonon lifetime. It is the presence of the Brillouin peak in the microwave-frequency regime, together with its wide-band tunability and narrow linewidth, which makes the interaction appropriate for applications ranging from ultra-narrow-linewidth lasers to microwave photonic filters; these applications are discussed in Sections 4 and 5.

The strategies employed to achieve efficient Brillouin interactions within integrated guided-wave systems vary dramatically depending on waveguide dimension, material properties, and the type of scattering process one seeks to utilize (See Figure 2 for different geometries). The central quantity that one seeks to optimise is the Brillouin gain G_B, given in units of $\mathrm{m}^{-1}\mathrm{W}^{-1}$. In general, it is necessary to use full-vectorial numerical methods to accurately predict the Brillouin gain [34], and this computation can be performed using commercial numerical solvers [34] or open source numerical tools [35,36]. However, in the limit when the waveguide dimensions are larger than the wavelength of light, one can obtain a rough estimate of the gain using a simplified model based on bulk electrostrictive properties, the elastic properties of the waveguide material, and the waveguide dimensions (see Box 2). In addition to the gain, a useful measure of the strength of the interaction is given by the Brillouin figure of merit $F = G_B PL$, in which L is the effective waveguide length, and P is the pump optical power within the waveguide. An additional practical consideration arises when attempting to induce SBS in semiconductor materials: two-photon absorption can lead to the production of free carriers that introduce additional nonlinear losses. These nonlinear losses impose some practical limits on the power handling of semiconductor waveguides. As a consequence, the realizable gain becomes highly dependent on the linear loss, free carrier lifetime, and waveguide dimensions, giving rise to a nontrivial design space for Brillouin gain in semiconductors[37]. Key material properties, as well as figures of merit that can be used to estimate the material contribution to the gain, are included in Table AA for several material systems. In most use-cases, we seek a scenario where (1) Brillouin nonlinearities are at least as large as competing nonlinear effects (e.g. Kerr and Raman) and (2) waveguide losses (linear and nonlinear) are low enough to permit a measureable Brillouin response. We use these basic criteria to guide our exploration of different material systems and the distinct advantages they have for specific applications.

3. Brillouin-active waveguides

Fig. 3a plots the measured gain vs loss for different Brillouin active waveguides and Fig. 3b plots the waveguide gain (in 1/m/W). A full table of experimental measurements in integrated systems is given in Table BB. The first experimental demonstration of SBS in an integrated waveguide was reported by Pant *et al.*[24] who used a chalcogenide As_2S_3 [38] rib waveguide in a photonic chip. This device had several features that enabled a large Brillouin gain factor: the high contrast in the optical and acoustic velocities in the core and cladding, which provided simultaneous optical and acoustic confinement and thus a large acousto-optic mode overlap, and a small optical mode area A (2.3 μm^2) compared to that of optical fibre (~85 μm^2 for single-mode fibre[17]). These factors, combined with the large refractive index and photoelasticity of As_2S_3, resulted in a value of G_B nearly 100 times that of silica optical fibre. The high gain, good power handling (> 500 mW), and low optical losses (typically 0.2-0.5 dB/cm) supported by such As_2S_3 waveguides have enabled large on/off gains (52 dB, corresponding to ~40 dB net gain) [39,40]. Further demonstrations highlighted that the Brillouin process can be selectively enhanced or inhibited using photonic bandgap structures [41]. Since this system supports the same nonlinear wave-

scattering geometry as optical fibres, many of the techniques of Brillouin-based signal processing developed in fibres are directly applicable to this chalcogenide waveguide platform [42,43].

While these first experimental systems utilized the intrinsic photoelastic response of the waveguide core to produce strong Brillouin coupling [42], it was also discovered that new mechanisms for Brillouin coupling emerge when light is confined below the optical wavelength-scale [21,34,44,45]. Such interactions, which result from the strong interaction of light with waveguide boundaries, become particularly important within high-index contrast waveguides having small cross-sections. For these waveguides two important effects come into play: first, phonon-induced boundary deflection modifies the local refractive index distribution (because a portion of the waveguide material is replaced with the surrounding material or free space), and second: large boundary forces can be generated by the radiation pressure arising from the interfering optical waves [21]. These two effects are in fact closely related, in the same way as the bulk effects of electrostriction and photoelasticity are related[17]. A full-vector formulation and careful accounting now becomes essential to correctly capture these forces to evaluate the Brillouin gain in waveguides that produce wavelength-scale confinement of light [34,44,45]. Radiation pressure has been extensively studied as a means of manipulating mechanical objects in the context of cavity optomechanics [46], and radiation pressure forces have also been used to drive strong optomechanical nonlinearities in "nanoweb" Photonic Crystal Fibre (PCF) geometries [47]. These same forces also offer a means of inhibiting the SBS process through a cancellation of optical forces [48], and it is certain that radiation pressure will play a dominant role in many integrated Brillouin photonics systems [25,26].

The realisation that radiation pressure could strongly modify Brillouin interactions was central to a key advance in this field: the demonstration of SBS in silicon and silicon-on-insulator (SOI) platforms, which are compatible with modern CMOS nanofabrication facilities. It is perhaps counterintuitive that conventional nanoscale SOI waveguides, which greatly enhance third-order Kerr and Raman nonlinearities [49], do not produce efficient Brillouin nonlinear interactions. Two effects cause the reduction of SBS in SOI waveguides. First, the photoelastic tensor component (p_{12}) that ordinarily produces backwards-SBS interactions (through coupling between transversely electromagnetic fields and longitudinal acoustic waves) is very small in silicon – about 16 times smaller than silica (see Table AA). Second, since silicon is a relatively stiff material, the sound velocity in a silicon core greatly exceeds that of the silica cladding. This means that a conventional SOI waveguide is anti-guiding for sound; consequently, generated sound-fields typically radiate into the substrate of such waveguides before appreciable light-sound scattering can occur [21,50 23]. However recent experiments have shown that have these problems can be solved by harnessing radiation pressure, together with coupling to different photoelastic tensor components, in suspended or quasi-suspended waveguide geometries (see Fig. Y). These waveguides use either an air cladding [25,41], thin pedestal [26], or a phononic crystal cladding [52] to reduce or eliminate the leakage of sound waves into the substrate. Since both radiation pressure and the dominant photoelastic tensor component of silicon (p_{11}) preferentially couple to transverse elastic wave motion, these silicon waveguides produce strong forward stimulated Brillouin scattering. It should

be noted that such forward Brillouin interactions produce energy transfer and coupled-wave dynamics that are quite different from the backwards SBS process common in optical fibres [25,51,53]. The intriguing dynamics, and the potential technological benefits, of such forward-scattering interactions were first demonstrated in microstructured fibre systems that employed similar confinement strategies [54,55]. Silicon Brillouin waveguide systems have produced record forward-SBS gain coefficients using sub-wavelength modal confinement [26], as well as net amplification at modest (5 mW) optical powers using low loss (<0.2 dB/cm) larger mode-area waveguides [51] that more effectively manage nonlinear losses. Such waveguide systems have enabled robust on/off gain (6.9 dB) corresponding to ~5.2 dB of net gain in a traveling-wave configuration [51] and more dramatic on/off gain (30 dB) corresponding to ~20 dB of net gain within resonant device configurations [56].

Recent studies have also utilized large-mode-area or 'dilute' silicon nitride waveguides to demonstrate appreciable Brillouin nonlinearities in the absence of acoustic wave guidance[33]. This is possible because, as the mode area of an optical waveguide increases, the necessity for acoustic guidance becomes relaxed [23]. In other words, acoustic wave guidance is only essential if the diffraction length of the sound-field is significantly shorter than the attenuation length. Because the attenuation length of high frequency (10 GHz) sound waves is typically less than 100 microns, one can see that—in the limit of large mode-area—appreciable Brillouin coupling is possible in the absence of acoustic guidance. In fact, the dilute silicon nitride waveguides of Ref. [33] produced appreciable Brillouin gain despite the fact that it is anti-guiding for sound. Similar results are also seen in quartz fibres, which have an undoped silica core that produces anti-guiding for sound [57]. While the gain values produced by such large mode area waveguides are modest in comparison to their high index chalcogenide and silicon counterparts (see Table BB, Fig. 3), the ultra-low losses (0.04 dB/cm) and high-power handling supported by these waveguides open up a range of complementary opportunities in the context of laser-physics, sensing, and metrology.

Looking beyond the experimentally demonstrated systems discussed above, a number of other material systems and waveguide geometries have been proposed for harnessing SBS at different wavelengths and for specific applications. In contrast to the acoustically-leaky rib-like guides in Ref. [33], CMOS-compatible silicon nitride suspended waveguides have been proposed for high-gain forward SBS devices [58,59]. In the mid-infrared, germanium is an extremely promising material for SBS, since it is softer and of higher index than silica glass, as well as being transparent across an extremely broad wavelength range. Germanium waveguides with silica substrate are predicted to exhibit high SBS gains at 4.0 μm [60]. Conversely, in the visible spectrum materials such as AlGaN have been proposed as compact SBS sources [61]. Aluminium nitride is an excellent material for opto-mechanical interactions since it has a very large acoustic lifetime and also because acoustic waves can be directly excited electronically: experiments demonstrating Brillouin scattering from induced acoustic waves have recently been

reported[15]. More exotic platforms have been proposed, and SBS in a suspended 3 mm long suspended graphene microfiber has recently been experimentally demonstrated[62].

Box 1 | Overview and types of Brillouin Scattering

One of three general types of stimulated Brillouin scattering processes may be dominant in a given structure, depending on the polarization of the optical fields [34,63] as well as waveguide material properties and geometry: These are (1) backward-SBS, (2) forward-SBS, and (3) inter-modal SBS. Backward scattering (Fig Xa) involves counter-propagating optical waves, and hence large-wavenumber acoustic modes, which have strong variation in strain along the waveguide direction; Forward scattering (Fig Xb) involves coupling of co-propagating optical modes to acoustic modes: for forward scattering the acoustic modes exist near the $q = 0$ point, at which the acoustic modes no longer propagate along the waveguide axis; these modes tend to have strong transverse components. Intermodal scattering (Fig Xc) involves acoustically-driven transitions between different optical modes and can occur in either the forward or backward direction. Regardless of the type of scattering, conservation of energy and momentum leads to strict phase-matching requirements on the interaction (Fig Xa-c). For optical modes of frequency ω_p and ω_s and wavenumbers $k_p$and k_s the acoustic mode must have frequency $\Omega = \omega_p - \omega_s$ and wavenumber $q = k_p - k_s$, as well as the appropriate symmetry to support the interaction [34,63]. These distinct phase matching conditions yield different sets of coupled wave equations with unique dynamics [21,45].

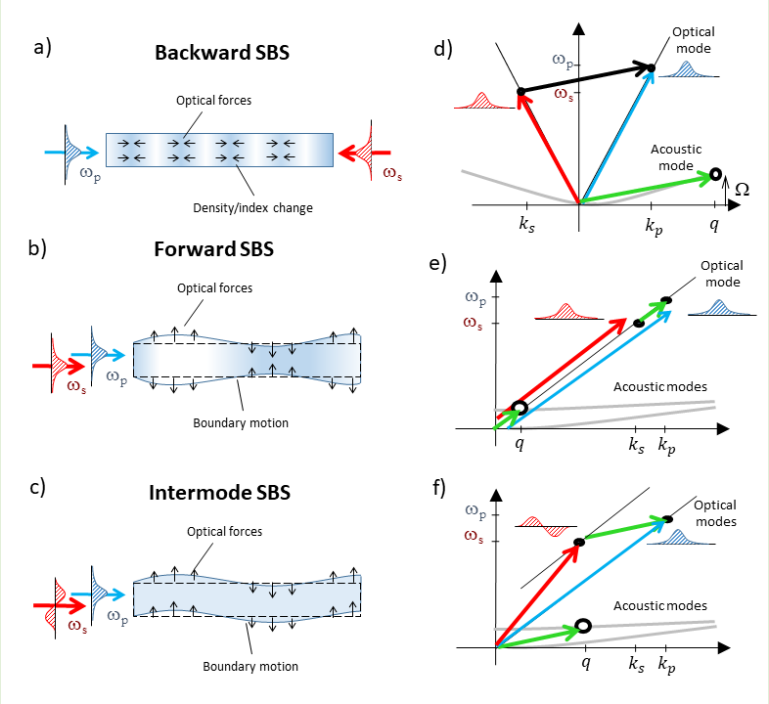

Fig. X: Types and mechanisms of Brillouin scattering; forces and scattering for (a) Backwards SBS; (b) Forward Brillouin scattering; and (c) and Intermode Brillouin scattering; dispersion curves showing the phase matching for backwards (d), forward (e) and intermode

Box 2 | Brillouin Gain and conditions

Acoustic mode confinement and control: For maximum Brillouin gain, both optical and acoustic waves should be confined in the same region. Confinement of the acoustic field can be achieved using isolation or suspension of the waveguide, or by total internal reflection (TIR), which occurs when the modal phase velocity is less than the velocity of the lowest-frequency waves (either shear or Rayleigh waves) in the surrounding substrate. If the TIR condition is not met or if the waveguide is insufficiently isolated then energy will be lost (Fig. Y), leading to a low quality factor Q and reduced gain.

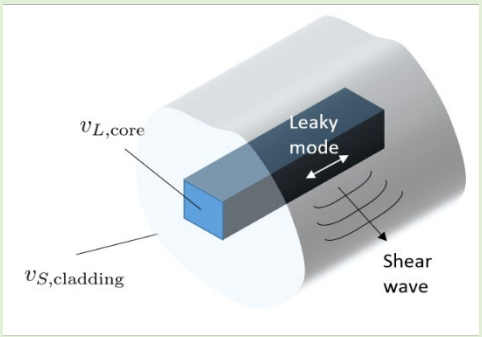

Fig. Y: A leaky acoustic mode will radiate and lose energy via the substrate – these waves are typically shear or Rayleigh waves.

Brillouin Gain: The Brillouin gain can be evaluated from the field profiles of the interacting *pump* and *Stokes* optical waves ($\boldsymbol{E}^P$ and $\boldsymbol{E}^S$ respectively), and the elastic displacement [64] profiles ($\boldsymbol{u}$) associated with the Brillouin active phonon modes. When the optical waveguide also supports acoustic wave guidance, a single Brillouin-active guided mode may suffice to describe the coupling, but when the acoustic waves rapidly dissipate (or if the waveguide is anti-guiding for sound) a continuum of phonon modes may be necessary[23,33,65]. When a single mode dominates, the Brillouin gain is [21,45]

$$G_B = \frac{2\omega_p Q}{\Omega_B^2 v_{gs} v_{gp}} |\langle \boldsymbol{f}, \boldsymbol{u} \rangle|^2 , \qquad (1)$$

where $\boldsymbol{f}$ is the generalized form of optical force density, arising from electrostriction and radiation pressure, produced by the interacting optical fields, v_{gp} (v_{gs}) is the group velocity of the pump (Stokes) wave, and Ω_B and Q are the frequency and quality factor of the acoustic mode. The contribution to the gain is largely governed by the degree of optical confinement[21]: when the waveguide dimension is of the order of the optical wavelength, radiation pressure becomes as large as electrostriction.

Material requirements: For backward-SBS, coupling is typically mediated by a single longitudinal acoustic mode; this means that the electrostrictive component of the gain is almost entirely determined by the p_{12} component of the photoelastic tensor (see Table Y). In the limit when the lateral waveguide dimensions are larger than the optical wavelength, the backward-SBS gain can be approximated as $G_B^{BSBS} = \omega n^6 p_{12}^2 Q/(2c^2 \rho v_a^2 A)$, where n and ρ are the waveguide refractive index and material density respectively, and A is the area of the waveguide cross-section. Multiplication by A produces the gain coefficient (in units of m/W) for widely-studied backward SBS processes in bulk materials [4,14]. Through forward-SBS, the coupling is determined by the p_{11} component, leading to an approximate gain of $G_B^{FSBS} = \omega n^6 p_{11}^2 Q/(\pi^2 c^2 \rho v_a^2 A)$. To arrive at this expression we have considered only coupling to the fundamental elastic wave formed by the free-motion of the waveguide boundaries in air, and many nontrivial aspects of the elastic wave physics have been discarded. A list of commonly-used platforms with approximate gains is given in Table Y.

4. Brillouin-active Resonators and Laser Oscillators

Racetrack and whispering-gallery resonators can also be used to obtain enormous enhancements to Brillouin gain, with resonant enhancement adding to any effects arising from the modal confinement. The enhancement of nonlinear effects remains a key driver for the development of high-finesse optical resonators [66] in photonics, and in these structures the quality factor can routinely exceed 10^{10}, with strong implications for SBS lasing. The current state-of-the-art in Brillouin-active resonators consists of a diverse range of geometries including planar rings or discs, microtoroids, and spherical whispering-gallery resonators (see Fig. 2). In Brillouin resonators, the pump optical finesse contributes to a resonant enhancement of pump power, while the finesse of the scattered optical mode (either Stokes or anti-Stokes depending on the configuration) corresponds to the increased optical path length over which the nonlinear interaction takes place [44] . Resonance-induced reduction of the SBS lasing threshold was first observed in fibre rings [18], while the first demonstration that geometric effects can significantly modify the SBS frequency and lasing threshold came from experiments in aerosolized liquid microdroplets [67]. In droplets, the SBS enhancement was ascribed to an effective wavevector spread of the pump caused by the focusing from the droplet face, in addition to resonant feedback from the droplets acting as low-Q optical cavities that support both the pump and Stokes frequencies. In spite of extensive developments on ultrahigh-Q microresonator systems in the 2000's, backward SBS was not observed in these systems until 2009 due to the difficulty in frequency-matching the multiple optical and mechanical modes. Ultralow-threshold SBS lasing and cascades were finally achieved in polished fluorite resonators whose FSR matched the SBS frequency[29], and with the use of high-order optical modes in much smaller reflowed silica microresonators [30]. Lasing thresholds as low as 3 μW were reported in these resonators[29]. On-chip resonant Brillouin lasing required an innovation in nanofabrication methods in order to precisely match the free-spectral-range of the Whispering-Gallery-Mode (WGM) cavity to the Stokes shift; this degree of precision was first realised in ultrahigh-Q silica-on-silicon wedge resonators [31], and the resulting technology has since enabled on-chip microwave synthesis [68] and Brillouin gyroscopes [69]. In spite of the resonant enhancement, the Brillouin frequency and strength of the Brillouin gain in these systems are determined by the same principles that govern SBS in bulk media.

Ultralow threshold *forward* SBS, which allowed access to high-coherence long-wavelength phonons, has also been observed in silica microresonators with the help of high-order optical modes [70]. The increased phonon lifetimes have enabled demonstrations of chiral cooling [32,65] and efficient nonreciprocal processes [71,72] (see Section 5). An important distinction is the very large phonon wavelengths in these systems relative to backward SBS, indicating that two types of geometric effects once again become significant. First, the phonons are confined by the curved resonator boundary, which acts to shape the mode spectrum, resulting in a diverse set of phase-matched phonon modes. Second, the mechanical deformation of the resonator boundary results in a radiation pressure contribution to the SBS gain [44].

Brillouin interactions are also the basis for a range of new chip-scale laser-oscillators with highly tailorable coherence properties (Fig 4f) and have been employed in a range of technologies from frequency combs [41] to microwave sources [68] and optical gyroscopes (rotation sensors) [69,73,74]. Brillouin laser oscillation occurs when an external pump-wave generates Brillouin gain that balances the round-trip losses within an optical resonator. Above threshold, a coherent optical Stokes wave builds from spontaneous noise to produce laser oscillation; through this process, incident pump photons are efficiently converted to an emitted optical Stokes wave. Within such systems, the coherence properties of the emitted Stokes wave—which are distinct from that of the pump—can be controlled by tailoring the three-wave dynamics of the system. In the case when the phonon loss rate is higher than the optical loss rate, the spectrum of the emitted optical Stokes wave exhibits Schawlow-Townes linewidth-narrowing for increasing laser powers. In this regime of operation, the linewidth of emitted Stokes wave can become extraordinarily narrow [75,76]. Conversely, in the case when the phonon loss rate is smaller than the optical loss rate, the linewidth of the intra-cavity phonon-field exhibits Schawlow-Townes linewidth-narrowing; this regime of oscillation is sometimes referred to as "phonon laser oscillation" [70,77]. In limit of vanishing phonon linewidth, the emitted optical Stokes wave can be viewed as a frequency shifted replica of the incident pump wave, meaning that the Stokes wave inherits the coherence properties of the pump wave. Both types of laser oscillation have been demonstrated in quasi-planar geometries, with Stokes oscillation realised using integrated chalcogenide [78–80], silica [81,82], silicon nitride [33], and phonon laser action demonstrated in both silica-on-silicon[77] and in silicon [83] waveguide platforms.

Brillouin lasers have numerous features that make them particularly desirable as the basis for compact low noise laser oscillators. For example, using the frequency selectivity provided by the narrow Brillouin gain bandwidth, a Brillouin laser can be designed to produce optical feedback for only a single longitudinal mode, eliminating sources of noise that result from mode competition [76]. Since the Brillouin interactions can be much stronger than other nonlinearities, the dynamics are captured by a relatively simple three-wave model [76,84]. These models reveal that phase fluctuations of the pump will be imprinted onto Stokes field, the acoustic field, or some combination thereof. When the phonon decay rate is greater than the Stokes optical decay rate, the acoustic-field is able to react to phase fluctuations of the pump on a much shorter time scale. As a result, the phase fluctuations of the pump are imprinted on the acoustic field while the Stokes field, which reacts on a much longer timescale, is effectively shielded from phase and amplitude fluctuations of the pump-wave. This process can yield Stokes laser emission that is orders of magnitude more spectrally pure than the pump [33,75,76,84,85]. Conversely, when the acoustic decay rate is lower than the Stokes optical decay rate, the Stokes mode follows the pump fluctuations, thereby shielding the acoustic mode and forming a spectrally pure phonon oscillation [70,77]. Building on this understanding, Brillouin lasers can be designed to produce Schawlow-Townes linewidth narrowing of either the optical field [33,85] or the phonon field [70,77,83] depending on the physical parameters of the system, most notably the relative size of the optical and acoustic decay rates. These devices can therefore be used for spectral purification, at the cost of introducing a small and readily corrected frequency shift onto the pump signal[85].

The optical linewidth-narrowing properties of Brillouin lasers are particularly promising as a means of generating laser sources with sub-Hz linewidths [75,84] . However, in practice, technical sources of noise that arise from the sensitivity of fibers to their environment typically limit the linewidth of Brillouin lasers [75]. Alternatively, the higher mode stabilities offered by integrated and ultra-compact Brillouin lasers can mitigate this problem, making it possible to demonstrate sub-Hz fundamental linewidths using ultra low loss silica [31,68], calcium fluoride[29], and dilute silicon nitride [33] photonic technologies. With further progress, ultra-narrow linewidth lasers could benefit applications ranging from frequency metrology, to sensing and coherent communications, and this has driven interest in chip-scale Brillouin laser oscillators in recent years. The prospect for high frequency microwave synthesizers also present a compelling opportunity for chip-scale Brillouin laser oscillator technologies [81].

5. Devices and applications

Harnessing SBS in centimetre-scale photonic chips is of significant interest for emerging integrated microwave photonics (MWP) techniques and optical communications, as well as for sensing and gyroscopes. Much research in this area is particularly motivated by the size, weight and power-consumption requirements of mobile and avionic platforms [86] , where on-chip Brillouin offers high-speed, low-weight and flexible solutions to several key problems in sensing and communications.

Photonics-assisted microwave systems (usually referred to as MWP) [86–88] form a well-established research field, providing key advantages of tailorable RF functionalities over frequency bandwidths which are not yet widely available in traditional electronic RF systems. Although commercial systems for multi-GHz bandwidth systems do exist, traditional RF devices have limited frequency range, degraded performance at high frequencies and lack wide tuning range; in addition, the size, weight and power consumption often prohibit their deployment on mobile platforms, such as drones. In particular, the coarse spectral resolution (typically of the order of GHz) of integrated optical systems typically struggle to meet the demanding requirements of many RF systems [89] which require filters with resolutions of the order of MHz as well as high frequency stability. Low-frequency acoustic waves have been used extensively in conventional signal processors where they enable narrow-band filters and delay lines for baseband and microwave frequencies[90], however simultaneously broadband GHz bandwidth and MHz resolution is unachievable in such systems. In the canonical MWP system, the frequency range is determined by the bandwidth of the electro-optic modulator and the detector; the linewidth of the signal processing function is determined by the photonic element, typically provided by a fibre Bragg grating, ring-resonator or the Brillouin effect [88]. Brillouin-based acousto-optic interactions offer a marriage between acoustic and optical signal processing, combining the broad bandwidth offered by photonics with the fine spectral resolution enabled by acoustics.

Reconfigurable microwave photonic filters: Of particular interest are photonic filter elements, which are key building blocks for all microwave systems. The Stokes gain in the SBS process forms the basis of an optical bandpass filter in a microwave photonic link [91,92], providing a broadly tunable microwave filter [85] with a resolution of about 10-30 MHz depending on the platform and material composition [94] (Fig 4a) .

Chip-based Brillouin MWP filters based on chalcogenide circuits have been extensively reported, producing narrowband (~ 30 MHz) [95] and broadband (500 MHz) [96] reconfigurable bandpass filter bandwidth, with ultra-wide frequency tunability over tens of gigahertz. To reduce the pump power consumption for ultra-high-extinction filters, Marpaung et al. reported low-power operation of a broadly tunable notch filter from 1-40 GHz using RF destructive interference, achieving an extinction of 60 dB and a reconfigurable resolution of 32–88 MHz[97,98]. Such a level of narrow spectral resolution, wideband frequency agility and flexible response tunability is challenging to achieve using other on-chip photonic devices such as ring resonators or periodic subwavelength structures, due to the limited quality factor of the resonance, the periodic spectral response and the resonantly enhanced nonlinearity that can distort the link performance. Recently, a novel integrated photonic-phononic emitter-receiver (PPER) device demonstrated a novel way to produce MWP bandpass filters with much sharper multi-pole filter shapes having spectral widths as narrow as 3 MHz [52]. This alternative device strategy yields reduced cross talk and noise from the optical pump due to the spatial separation of transmitter and receiver waveguides [99]. Brillouin based photonic filters have been implemented in coherent optical communication systems providing self-track optical filters for carrier recovery and improving performance of comb-based systems [100,101].

Microwave signal generation and measurement: The inherent narrow linewidth of the SBS gain resonance makes it a promising gain medium for optical and RF signal generation, without requiring additive doped materials (Fig 4b). A Brillouin active resonator with low optical loss can be made to lase above threshold (See Section 4); a cascading of the Brillouin process can result in the production of multiple spectral emission lines at the cavity resonances[68]. The interference between these lines can be used as an ultra-low phase-noise microwave source[68]. High-performance SBS-based microwave synthesizers are particularly promising in CMOS-compatible platforms, enabled by recent progress in on-chip SBS lasers in Si-As_2S_3 hybrid [80], Si_3N_4 [33] and pure silicon photonic circuits[51,83].

In addition to traditional Brillouin-based RF sources using optical cavities, embedding SBS in electrical-optic hybrid cavities to form optoelectronic oscillators (OEOs) can generate high-spectral-purity RF signals. The on-chip SBS gain can shorten the total cavity length, resulting in an increased mode spacing in the frequency domain. Therefore, the narrow-band SBS gain can select only one cavity mode to oscillate. The use of SBS eradicates the need for electrical filters, which severely limit the frequency tuning range [102].

Opto-acoustic data storage and delay components: The manipulation of signal time delay is crucial for microwave photonic signal processing, including radar beam pointing, signal synchronization and signal filtering in radio-frequency communication systems [103]. As a consequence of the Kramers-Kronig

relations, the Brillouin gain and loss resonances produce strong distortions in phase and group index [104], which can be exploited for manipulating the phase of a microwave signal, enabling broadband phase-shifts and delay lines, which are essential functions for dynamic beam-forming radar[88]. The dispersive phase response of SBS can also be applied to the signal spectrum, consisting of a range of frequency components, to generate relative time delays: for light, sound or microwaves[105]. Delay systems based on stimulated Brillouin scattering (SBS) operate at room temperature (in contrast with many EIT slow light systems that require cryogenic operation), can be implemented at telecommunications wavelengths, and can be fully controlled via the optical pump wave. Different approaches have been reported, including SBS slow-light [72,106–109], fibre delay lines based on Brillouin dynamic gratings [110,111], Brillouin quasi-light storage [112] and Brillouin-based light storage via photon-phonon conversion [113,114] (Fig 4c). Compared to the schemes based on integrated ring resonators and Bragg gratings, SBS enables continuous tuning, a flexible and programmable response over a wide frequency range, reduced structural complexity, and signal amplification due to the Brillouin gain response [115]. However, Brillouin-based slow light systems are limited in time delay to one or two pulse widths, corresponding to a delay time – bandwidth product of about 1[116]. This limitation can be overcome, for example by Brillouin-based light storage via photon-phonon conversion[115]: this technique involves using a powerful pump to convert an anti-Stokes signal into a Brillouin dynamic grating; the grating can then be ``read out'' at a later time which is limited only by the phonon lifetime in the waveguide[112]. Brillouin storage has been shown for bursts of pulses, however implementation for a continuous data stream is a significant challenge. While bandwidth limitations remain a challenge for delaying optical data streams, Brillouin delay is finding applications in analogue microwave photonics systems where the bandwidth requirements are more relaxed[117].

Isolators and non-reciprocal components: While modern integrated photonics already have optical component technologies for waveguiding, switching, modulation, frequency-shifting, light generation, and light detection, one critical class of components has not yet been fully realized: these are non-reciprocal devices, specifically optical isolators, circulators, and gyrators, which are essential in all photonic systems for enabling directional signal routing and protection functions. The key to achieving non-reciprocal operation is to break time-reversal symmetry in the medium [118], which in turn requires either magnetic fields (the dominant off-chip approach), time-variation of material properties, or nonlinearity. The magneto-optic approach remains difficult to implement on-chip due to fabrication challenges and lack of suitable materials. Non-reciprocities from traditional nonlinear effects are often narrow-band and have the drawback that the amount of isolation depends on the power in the signal. Brillouin scattering overcomes several of these disadvantages: SBS based isolators can be made broadband, depend linearly on the power of a pump that can be adjusted independently of the signal, can be employed in a large range of dielectrics and are compatible with integration technologies, which ultimately will allow for full integration of a range of optoelectronic functions.

Generally speaking, time-reversal symmetry can be broken in a medium by inducing spatio-temporal modulation of the local susceptibility, which mimics a momentum bias [119]. Brillouin scattering provides

two opportunities to produce such a momentum bias, through either the propagating acoustic wave or the propagating optical fields involved in the process. For instance, non-reciprocal optical gain is automatically produced in SBS since the phase-matching is dictated by the direction of the pump. This approach was first demonstrated in photonic crystal fibre by Kang et al.[120] However, the bandwidth of this configuration is limited by the linewidth of the SBS gain to 10s of MHz, too small for high-speed signal processing. Extensions of this approach have been implemented using whispering gallery mode cavities[71,72], enabling low power and small footprints, but again limited to ultra-narrow bandwidths. On the other hand, an acoustically-excited optical waveguide can enable inter-modal or inter-band optical coupling [121,122] over an extremely wide range of frequencies provided the optical mode dispersions are suitable. First proposed by Huang *et al.*[123], this scattering is strongly non-reciprocal due to the Brillouin phase-matching rules. A mode-splitter can then optionally be used to separate the modes, providing a basis for optical isolation. On-chip architectures were considered by Poulton et al., who examined the feasibility of dispersion engineering to further broaden the bandwidth [124]. Demonstrations of this form of nonreciprocity on-chip were recently reported by both direct acoustic pumping in an aluminium nitride resonator[15] and by an optically pumped SBS approach in a silicon waveguide [125] (Fig 4d). The waveguide method leverages long propagation lengths to produce nonreciprocal light propagation with high contrast (> 20 dB) over very high bandwidths (> 1 nm); however, new strategies to manage the effects of nonlinear absorption in silicon-based Brillouin devices will be required to push conversion efficiencies closer to unity. The resonator approach trades bandwidth for extreme compactness, and when used in a shunt or induced-transparency configuration [15,72,126], can also dramatically lower the optical insertion loss [127].

High spatial-resolution sensing: Since the SBS frequency shift is sensitive to environmental variables such as temperature [128] and strain [129] it has been adopted as a distributed sensing mechanism in long optical fibres to monitor critical structures such as buildings and bridges [130]. The spatial resolution required in structural health monitoring ranges from a few meters to a few cm depending on the application, which can be achieved using a distributed SBS measurement such as Brillouin optical time domain analysis (BOTDA) [128,131,132] and Brillouin optical correlation domain analysis (BOCDA) [133]. BOTDA is based on optical pump pulses whose duration determines the spatial resolution of the SBS response [134] and is therefore limited by the phonon lifetime. Fiber-based implementations based on time-domain techniques are already mature and used in some real-world applications. Distributed sensing for integrated optics on the other hand [135], which requires very high spatial resolution as the waveguides themselves are short, has only been recently reported with spatial resolution of sub-mm achieved, using BOCDA [136–138] (Fig 4e). Increasing the spatial resolution, hence allowing precise mapping of the waveguide structure, requires larger levels of SBS gain and would eventually enter the length scale on which the acoustic wave is propagating; a transient description of the distributed SBS response would likely be required [134]. New schemes that can “look” outside the fiber using distributed forward scattering have just recently been demonstrated and set a new paradigm in distributed fiber sensing [139,140]. However, large increases in the spatial resolution will be required to implement these schemes on chip.

RF frequency identification: Fast and accurate determination of multiple unknown RF signal frequencies over a wide RF frequency range is crucial for environment and threat awareness in modern defence applications, which is referred to as Instantaneous Frequency Measurement (IFM) technique [141] (Fig 4f). Traditional photonic techniques offer extended frequency measurement, however are limited by the trade-off between measurement accuracy and range determined by the optical filters. SBS combines the very narrow linewidth and high extinction over a wide RF frequency range, which allows for a large slope of power-to-frequency mapping function; such a large mapping slope enables the unambiguous estimation of RF frequencies with an ultra-low error of <1 MHz [142].

Optical gyroscopes: Ultra-narrow linewidth Brillouin lasers are the basis for a new breed of compact optical gyroscopes for sensing and navigation [74]. Most modern optical gyroscopes rely on the well-established Sagnac interferometer to sense rotation rates. However, these systems historically utilize bulky optical fibre spools or free-space resonators that are not practical for all applications [143]. Alternatively, by harnessing counterpropagating Brillouin lasers in a chip-based device, Vahala *et al.* measured the rotation of a Sagnac-induced frequency shift, demonstrating an on-chip gyroscope with a rotation-rate measurement that surpassed in-service rotation-sensing schemes by over 40-fold [69]. Using foundry-ready fabrication process, such chip-scale Brillouin-based gyroscope technologies have also been demonstrated using ultralow loss silicon nitride waveguides, demonstrating an alternative path towards large-scale integration of such technologies [74].

6. Outlook

Fig. 5 shows a conceptual illustration of a chip-scale integrated microwave/RF processor for broadband communications, incorporating distinct functionalities, enabled by strong on-chip opto-acoustic interactions. Although enormous progress has been made, significant challenges remain to be addressed for this new technology to have a pervasive impact in communications and sensing applications. For microwave photonic applications, there remain long-standing issues for Brillouin-based photonic processing associated with the amplification noise [144] which can significantly deteriorate the SNR and increase the noise figure of Brillouin-based MWP systems [145,146]. Achieving low-noise or noise-free Brillouin signal processing is a more fundamental and intriguing task. The excess amplification noise is induced by the interaction of the intense optical pump and the thermal acoustic phonons, generating incoherent scattered optical waves. This Amplified-Spontaneous-Emission (ASE)-like noise coincides with the signal of interest at Stokes frequency, leading to SNR degradation of signals within the SBS gain spectrum. Several techniques have been proposed to mitigate the high amplification noise in the Brillouin-based filter passbands, such as multi-stage Brillouin amplification [147], Brillouin filter schemes based on loss rather than gain [145,146] and spatially-separated signals in the Photonic–Phononic Emit–Receive (PPER) scheme [99]. It is expected that operating at cryogenic temperatures should reduce noise, but this will clearly complicate practical implementation. There remain challenges for on-chip SBS lasers to become useful in real world applications. For example, for atomic clock applications, microwave oscillators with sub-Hz linewidths are required. The key to achieving

ultranarrow linewidths is to ensure that the Schawlow-Townes linewidth is as small as possible; this requires ultrahigh Q-factors (100M-1B).

The above-mentioned optoelectronic devices enabled by on-chip SBS require isolation to inhibit back-reflections that damage detectors and corrupt device performance. The common goal for all nonreciprocal devices is to maximize bandwidth while maintaining extremely low insertion loss in at least one propagation direction. Fortunately, SBS provides an elegant scheme for broadband isolation that can be seamlessly integrated into the SBS chip. Initial reports are encouraging for on-chip integration of Brillouin-based isolators in a range of materials, but some limitations persist. In silicon, for instance, there is continued need device strategies that more effectively mitigate nonlinear absorption while boosting the Brillouin coupling strength to reduce device footprint. Simultaneously, the nonreciprocal contrast which is defined using relative transmission coefficients in the case of isolators and circulators, and relative phase shift for gyrators, must be maximized. From an engineering perspective, these devices should be made compact for ease of integration and replication and should employ near-zero input power to operate. All these goals could be simultaneously achieved with an increase of Brillouin gain, which controls the scattering rate that ultimately governs contrast, and also lowers the required pump power. Moreover, the "wall-plug" power efficiency with electrically- or acoustically-driven Brillouin scattering can be much better than with an optically-driven system. In this context, materials that simultaneously exhibit large acousto-optic coupling and very large electro-mechanical transduction efficiency (e.g. lithium niobate, aluminium nitride, and similar optical grade piezoelectrics) are a new frontier [148]. Tremendous new opportunities exist for innovative approaches that leverage acousto-optics and Brillouin phase-matching for nonreciprocal devices.

The numerous advances in fabrication, performance and application, have also of course required developments in theoretical frameworks and tools. SBS in integrated platforms has been addressed in a range of formulations including calculation of optical and elastic forces using stress tensors [21,34,149], coupled mode pictures avoiding forces [45], and Lagrangian [150] and Hamiltonian [151,152] formulations where the opto-elastic coupling is captured as interaction energy. Hamiltonian descriptions naturally allow a quantum formulation, which provides a mechanism for accounting for quantum noise as well as classical noise in SBS lasers and other active systems.[83] Clarifying the connections and analogies to localised opto-mechanical systems has also been fruitful [43,153], and waveguide symmetries have been found to be important [34,63] in understanding the gain, in a very similar fashion to the concept of Raman-active media. Finally, while to date most calculations have been done using a combination of commercial tools (typically COMSOL) and in-house codes, several open-source codes are now available. [35,154,155] This should foster increased validation of modelling by different groups and more efficient and convenient calculations for novel waveguide structures. There is enormous opportunity to extend theoretical work such as developing codes that can treat a broader range of structures, and the development of comprehensive noise models.

In this context, on-chip Brillouin is also providing new opportunities for fundamental studies. For example, phonon squeezing and entanglement is possible and is potentially the basis of quantum

memory [156]. The ability to manipulate photons using integrated circuits opens new possibilities for thermal engineering, leading to cooling of phononic modes [157] and the production of unidirectional thermal conductors – thermal diodes – which allow *heat* to flow in only one direction and are of great importance in energy research [158]. Recent demonstrations highlight parity symmetry breaking with Brillouin scattering [159], as the basis of the suppression of disorder-induced scattering and Rayleigh scattering of both light and sound in waveguides and resonators [160]. Other emerging forms of Brillouin scattering and Brillouin lasing have been postulated – for example there has been recent research on Brillouin scattering with magnons [161]. Finally, there exist better materials for harnessing the interaction, for example recent work suggests metamaterials can be used to manipulate photoelasticity, leading to possibilities for enhancing or inhibiting SBS [162].

We believe SBS is growing in importance for photonics applications and that the integration of Brillouin scattering offers great promise for a range of applications for deployment in the real world as well as being of fundamental importance.

Acknowledgements:

BE acknowledges support from Australian Research Council (ARC) Linkage grant (LP170100112) with Harris Corporation, AFOSR/AOARD (FA2386-16-1-4036) and the U.S. Office of Naval Research Global (ONRG) (N62909-18-1-2013). MJS, BJE and CP acknowledge the support of Australian Research Council (ARC) (Discovery Project DP160101691. GB acknowledges support of the Office of Naval Research Director of Research Early Career Grant N00014-17-1-2209 and National Science Foundation grant EFMA-1627184.

All authors contributed to the writing of this manuscript.

Competing Interests statement,

The authors declare no competing interests

References :

1. Brillouin, L. Diffusion de la lumière par un corps transparent homogène. *Ann. Phys. (Paris).* **17**, 88–122 (1922).
2. Mandelstam, L. I. Light scattering by inhomogeneous media. *Zh. Russ. Fiz-Khim.* **58**, 381–386 (1926).
3. Garmire, E. Perspectives on stimulated Brillouin scattering. *New J. Phys.* **19**, 011003 (2017).
4. Boyd, R. W. *Nonlinear optics*. (Academic, 2008).
5. Gross, E. Change of wavelength of light due to elastic heat waves at scattering in liquids. *Nature* **126**, 201–202 (1930).

6. Krishnan, R. S. The scattering of light in fused quartz and its Raman spectrum. *Proc. Indian Acad. Sci. - Sect. A* **37**, 377–384 (1953).

7. Krishnan, R. S. & Chandrasekharan, V. Thermal scattering of light in crystals - Part I: Quartz. *Proc. Indian Acad. Sci. - Sect. A* **31**, 427–434 (1950).

8. Krishnan, R. Thermal scattering of light in diamond. *Nature* **4048**, 740–741 (1947).

9. Chandrasekharan, V. Thermal scattering of light in crytals - Part III: Theory for birefringent crystals. *Proc. Indian Acad. Sci. - Sect. A* **33**, 183–198 (1951).

10. Chandrasekharan, V. Thermal scattering of light in crystals - Part II: Diamond. *Proc. Indian Acad. Sci. - Sect. A* **32**, 379 (1950).

11. Chiao, R., Townes, C. & Stoicheff, B. Stimulated Brillouin scattering and coherent generation of intense hypersonic waves. *Phys. Rev. Lett.* **12**, 592–596 (1964).

12. Garmire, E. & Townes, C. H. Stimulated brillouin scattering in liquids. *Appl. Phys. Lett.* **5**, 84–86 (1964).

13. Williams, R. J. *et al.* Diamond Brillouin Lasers. *arxiv* 1807.00240 (2018).

14. Agrawal, G. P. *Nonlinear Fiber Optics*. (Academic, 2012).

15. Sohn, D. B., Kim, S. & Bahl, G. Time-reversal symmetry breaking with acoustic pumping of nanophotonic circuits. *Nat. Photonics* **12**, 91–97 (2018).

16. Ippen, E. P. & Stolen, R. H. Stimulated Brillouin scattering in optical fibers. *Appl. Phys. Lett.* **21**, 539–541 (1972).

17. Kobyakov, A., Sauer, M. & Chowdhury, D. Stimulated Brillouin scattering in optical fibers. *Adv. Opt. Photonics* **2**, 1–59 (2010).

18. Hill, K. O., Kawasaki, B. S. & Johnson, D. C. CW Brillouin laser. *Appl. Phys. Lett.* **28**, 608–609 (1976).

19. Dainese, P. *et al.* Stimulated Brillouin scattering from multi-GHz-guided acoustic phonons in nanostructured photonic crystal fibres. *Nat. Phys.* **2**, 388–392 (2006).

20. Beugnot, J.-C., Sylvestre, T., Maillotte, H., Mélin, G. & Laude, V. Guided acoustic wave Brillouin scattering in photonic crystal fibers. *Opt. Lett.* **32**, 17–19 (2007).

21. Rakich, P. T., Reinke, C., Camacho, R., Davids, P. & Wang, Z. Giant Enhancement of Stimulated Brillouin Scattering in the Subwavelength Limit. *Phys. Rev. X* **2**, 011008 (2012).

22. Nikles, M., Thevenaz, L. & Robert, P. A. Brillouin gain spectrum characterization in single-mode optical fibers. *J. Light. Technol.* **15**, 1842–1851 (1997).

23. Poulton, C. G., Pant, R. & Eggleton, B. J. Acoustic confinement and stimulated Brillouin scattering in integrated optical waveguides. *J. Opt. Soc. Am. B* **30**, 2657–2664 (2013).

24. Pant, R. *et al.* On-chip stimulated Brillouin scattering. *Opt. Express* **19**, 388–392 (2011).

25. Shin, H. *et al.* Tailorable stimulated Brillouin scattering in nanoscale silicon waveguides. *Nat.*

Commun. **4**, 1944 (2013).

26. Van Laer, R., Kuyken, B., Van Thourhout, D. & Baets, R. Interaction between light and highly confined hypersound in a silicon photonic nanowire. *Nat. Photonics* **9**, 199–203 (2015).

27. Yang, K. Y. *et al.* Bridging ultrahigh-Q devices and photonic circuits. *Nat. Photonics* **12**, 297–302 (2018).

28. Minardo, A., Bernini, R., Amato, L. & L. Zeni. Bridge monitoring using brillouin fiber-optic sensors. *IEEE Sens. J.* **12**, 145–150 (2011).

29. Grudinin, I. S., Matsko, A. B. & Maleki, L. Brillouin Lasing with a CaF2 Whispering Gallery Mode Resonator. *Phys. Rev. Lett.* 043902 (2009).

30. Tomes, M. & Carmon, T. Photonic micro-electromechanical systems vibrating at X-band (11-GHz) rates. *Phys. Rev. Lett.* **102**, 113601 (2009).

31. Lee, H. *et al.* Chemically etched ultrahigh-Q wedge-resonator on a silicon chip. *Nat. Photonics* **6**, 369–373 (2012).

32. Bahl, G., Tomes, M., Marquardt, F. & Carmon, T. Observation of spontaneous Brillouin cooling. *Nat. Phys.* **8**, 203–207 (2012).

33. Gundavarapu, S. *et al.* Sub-hertz fundamental linewidth photonic integrated Brillouin laser. *Nat. Photonics* **13**, 60–67 (2019).

34. Qiu, W., Rakich, P., Shin, H. & Dong, H. Stimulated Brillouin scattering in nanoscale silicon step-index waveguides: a general framework of selection rules and calculating SBS gain. *Opt. Express* **21**, 31402–31419 (2013).

35. Sturmberg, B. C. P. *et al.* NumBAT: The integrated, open source Numerical Brillouin Analysis Tool. *arxiv* 1811.10219 (2018).

36. M. Malinowski, S. F. Devices, Physics and Simulation of Optoelectronic. in *Proc. SPIE XXVII* doi:10.1117/12.2509738 (2019).

37. Wolff, C., Gutsche, P., Steel, M. J., Eggleton, B. J. & Poulton, C. G. Impact of nonlinear loss on stimulated Brillouin scattering. *J. Opt. Soc. Am. B* **32**, 1968 (2015).

38. Eggleton, B. J., Luther-Davies, B. & Richardson, K. Chalcogenide photonics. *Nat. Photonics* **5**, 141–148 (2011).

39. Choudhary, A. *et al.* Advanced Integrated Microwave Signal Processing with Giant On-Chip Brillouin Gain. *J. Light. Technol.* **35**, 846–854 (2017).

40. Aryanfar, I. *et al.* Chip-based Brillouin radio frequency photonic phase shifter and wideband time delay. *Opt. Lett.* **42**, 1313–1316 (2017).

41. Merklein, M. *et al.* Enhancing and inhibiting stimulated Brillouin scattering in photonic integrated circuits. *Nat. Commun.* **6**, 6396 (2015).

42. Eggleton, B. J., Poulton, C. G. & Pant, R. Inducing and harnessing stimulated Brillouin scattering in photonic integrated circuits. *Adv. Opt. Photonics* **5**, 536 (2013).

43. Safavi-Naeini, A. H., Thourhout, D. Van, Baets, R. & Laer, R. Van. Controlling phonons and photons at the wavelength scale: integrated photonics meets integrated phononics. *Optica* **6**, 213–232 (2019).

44. Dostart, N., Kim, S. & Bahl, G. Giant gain enhancement in surface-confined resonant Stimulated Brillouin Scattering. *Laser Photonics Rev.* **9**, 689–705 (2015).

45. Wolff, C., Steel, M. J., Eggleton, B. J. & Poulton, C. G. Stimulated Brillouin scattering in integrated photonic waveguides: forces, scattering mechanisms and coupled mode analysis. *Phys. Rev. A* **92**, 013836:1–13 (2015).

46. Aspelmeyer, M., Kippenberg, T. J. & Marquardt, F. Cavity optomechanics. *Rev. Mod. Phys.* **86**, 1391–1452 (2014).

47. Butsch, A. *et al.* Optomechanical nonlinearity in dual-nanoweb structure suspended inside capillary fiber. *Phys. Rev. Lett.* **109**, 183904:1–5 (2012).

48. Florez, O. *et al.* Brillouin scattering self-cancellation. *Nat. Commun.* **7**, 11759:1–8 (2016).

49. Leuthold, J., Koos, C. & Freude, W. Nonlinear silicon photonics. *Nat. Photonics* **4**, 535–544 (2010).

50. Qiu, W., Rakich, P. T., Soljacic, M. & Wang, Z. Stimulated brillouin scattering in nanoscale silicon step-index waveguides: A general framework of selection rules and calculating SBS gain. **21**, 276–280 (2012).

51. Kittlaus, E. A., Shin, H. & Rakich, P. T. Large Brillouin amplification in silicon. *Nat. Photonics* **10**, 463–467 (2016).

52. Shin, H. *et al.* Control of coherent information via on-chip photonic–phononic emitter–receivers. *Nat. Commun.* **6**, 6427 (2015).

53. Kittlaus, E. A., Otterstrom, N. T. & Rakich., P. T. On-chip inter-modal Brillouin scattering. *On-chip inter-modal Brillouin Scatt.* **8**, 15819 (2017).

54. Kang, M. S., Nazarkin, A., Brenn, A. & Russell, P. S. J. Tightly trapped acoustic phonons in photonic crystal fibres as highly nonlinear artificial Raman oscillators. *Nat. Phys.* **5**, 276–280 (2009).

55. Kang, M., Brenn, A. & St.J. Russell, P. All-optical control of gigahertz acoustic resonances by forward stimulated interpolarization scattering in a photonic crystal fiber. *Phys. Rev. Lett.* **105**, 153901 (2010).

56. Otterstrom, N. T., Kittlaus, E. A., Gertler, S., Behunin, R. O. & Anthony L. Lentine, P. T. R. Resonantly enhanced nonreciprocal silicon Brillouin amplifier. *arXiv Prepr. arXiv* **1903.03907**, (2019).

57. Dragic, P., Law, P.-C., Ballato, J., Hawkins, T. & Foy, P. Brillouin spectroscopy of YAG-derived optical fibers. *Opt. Express* **18**, 10055–10067 (201AD).

58. Dehghannasiri, R., Eftekhar, A. A. & Adibi, A. Raman-like stimulated Brillouin scattering in phononic-crystal-assisted silicon-nitride waveguides. *Phys. Rev. A* **96**, 053836 (2017).

59. Dehghannasiri, R., Eftekhar, A. A. & Adibi, A. Observation of Stimulated Brillouin Scattering in Si3N4 waveguides. in *IEEE Photonics Conference* 135–136 (2017). doi:10.1007/s13398-014-0173-7.2

60. Wolff, C., Soref, R., Poulton, C. G. & Eggleton, B. J. Germanium as a material for stimulated Brillouin scattering in the mid-infrared. *Opt. Express* **22**, 30735 (2014).

61. De Leonardis, F., Soref, R. A., Soltani, M. & Passaro, V. M. N. Stimulated Brillouin Scattering in an AlGaN Photonics Platform Operating in the Visible Spectral Range. *Sci. Rep.* **8**, 14849:1–13 (2018).

62. Zhu, J. *et al.* Stimulated Brillouin scattering induced all-optical modulation in graphene microfiber. *Photonics Res.* **7**, 8–13 (2019).

63. Wolff, C., Steel, M. J. & Poulton, C. G. Formal selection rules for Brillouin scattering in integrated waveguides and structured fibers. *Opt. Express* **22**, 32489 (2014).

64. Auld, B. A. *Acoustic Fields and Waves in Solids*. (Krieger Publishing Company, 1990).

65. Kim, S., Xu, X., Taylor, J. M. & Bahl, G. Dynamically induced robust phonon transport and chiral cooling in an optomechanical system. *Nat. Commun.* **8**, 205:1–7 (2017).

66. Vahala, K. J. Microcavities Optical. *Nature* **424**, 839–846 (2003).

67. Zhang, J.-Z. & Chang, R. K. Generation and suppression of stimulated Brillouin scattering in single liquid droplets. *J. Opt. Soc. Am. B* **6**, 151 (1989).

68. Li, J., Lee, H. & Vahala, K. J. Microwave synthesizer using an on-chip Brillouin oscillator. *Nat. Commun.* **4**, 2097 (2013).

69. Li, J., Suh, M.-G. & Vahala, K. Microresonator Brillouin gyroscope. *Optica* **4**, 346 (2017).

70. Bahl, G., Zehnpfennig, J., Tomes, M. & Carmon, T. Stimulated optomechanical excitation of surface acoustic waves in a microdevice. *Nat. Commun.* **2**, 403–406 (2011).

71. Kim, J., Kuzyk, M. C., Han, K., Wang, H. & Bahl, G. Non-reciprocal Brillouin scattering induced transparency. *Nat. Phys.* **11**, 275–280 (2015).

72. Dong, C. H. *et al.* Brillouin-scattering-induced transparency and non-reciprocal light storage. *Nat. Commun.* **6**, 6193 (2015).

73. Sanders, G. A. *et al.* Fiber optic gyro development at Honeywell. in *Fiber Optic Sensors and Applications XIII* 985207 (2016).

74. Gundavarapu, S. *et al.* Interferometric Optical Gyroscope Based on an Integrated Si3N4 Low-Loss Waveguide Coil. *J. Light. Technol.* **36**, 1185–1191 (2018).

75. Smith, S. P., Zarinetchi, F. & Ezekiel, S. Narrow-linewidth stimulated Brillouin fiber laser and applications. *Opt. Lett.* **16**, 393–395 (1991).

76. Debut, A., Randoux, S. & Zemmouri, J. Linewidth narrowing in Brillouin lasers: Theoretical analysis. *Phys. Rev. A* **62**, 023803 (2000).

77. Grudinin, I. S., Lee, H., O. Painter, A. & Vahala, K. J. Phonon Laser Action in a Tunable Two-Level System. *Phys. Rev. Lett.* **104**, 083901 (2010).

78. Kabakova, I., Marpaung, D., Poulton, C. & Eggleton, B. Harnessing On-Chip SBS. *Optics and Photonics News* 34–39 (2015).

79. Kabakova, I. V. *et al.* Narrow linewidth Brillouin laser based on chalcogenide photonic chip. *Opt. Lett.* **38**, 3208 (2013).

80. Morrison, B. *et al.* Compact Brillouin devices through hybrid integration on Silicon. **4**, 847–854 (2017).

81. Li, J., Lee, H. & Vahala, K. J. Low-noise Brillouin laser on a chip at 1064 nm. *Opt. Lett.* **39**, 287 (2014).

82. Loh, W. *et al.* Dual-microcavity narrow-linewidth Brillouin laser. *Optica* **2**, 225 (2015).

83. Otterstrom, N. T., Behunin, R. O., Kittlaus, E. A., Wang, Z. & Rakich, P. T. A silicon Brillouin laser. *Science (80-.).* **360**, 1113–1116 (2018).

84. Le Floch, S. & Cambon, P. Theoretical evaluation of the Brillouin threshold and the steady-state Brillouin equations in standard single-mode optical fibers. *J. Opt. Soc. Am. A* **20**, 1132 (2003).

85. Li, J., Lee, H., Tong Chen, A. & Vahala, K. J. Characterization of a high coherence, Brillouin microcavity laser on silicon. *Opt. Express* **20**, 20170–20180 (2012).

86. Marpaung, D., Yao, J. & Capmany, J. Integrated microwave photonics. *Nat. Photonics* **13**, 80–90 (2019).

87. Seeds, A. J. & Williams, K. J. Microwave photonics. *J. Light. Technol.* **24**, 2628–4641 (2006).

88. Capmany, J. & Novak, D. Microwave photonics combines two worlds. *Nat. Photonics* **1**, 319–330 (2007).

89. Capmany, J., Ortega, B. & Pastor, D. A tutorial on microwave photonic filters. *J. Light. Technol.* **24**, 201–229 (2006).

90. Campbell, C. *Surface Acoustic Wave Devices for Mobile and Wireless Communications*. (Academic Press, 1998).

91. B. Vidal, M. A. Piqueras, J. M. Tunable and reconfigurable photonic microwave filter based on stimulated Brillouin scattering. *Opt. Lett.* **32**, 23–25 (2007).

92. Juan Sancho; Sanghoon Chin; *et al.* Dynamic Microwave Photonic Filter Using Separate Carrier Tuning Based on Stimulated Brillouin Scattering in Fibers. *IEEE Photonics Technol. Lett.* **22**, 1753–1755 (2010).

93. Zhang, W. & Minasian, R. A. Widely tunable single-passband microwave photonic filter based on stimulated Brillouin scattering. *IEEE Photon. Technol. Lett.* **23**, 1775–1777 (2011).

94. Pant, R. *et al.* On-chip stimulated Brillouin Scattering for microwave signal processing and generation. *Laser Photon. Rev.* **8**, 653–666 (2014).

95. Fan, S. *et al.* Photonic chip based tunable and reconfigurable narrowband microwave photonic filter using stimulated Brillouin scattering. *Opt. Express* **20**, 18836 (2012).

96. Choudhary, A. *et al.* Tailoring of the Brillouin gain for on-chip widely tunable and reconfigurable broadband microwave photonic filters. *Opt. Lett.* **41**, 436 (2016).

97. Marpaung, D. *et al.* Low-power, chip-based stimulated Brillouin scattering microwave photonic filter with ultrahigh selectivity. *Optica* **2**, 76 (2015).

98. Marpaung, D., Pagani, M., Morrison, B. & Eggleton, B. J. Nonlinear integrated microwave photonics. *J. Light. Technol.* **32**, (2014).

99. Kittlaus, E. A., Kharel, P., Otterstrom, N. T., Wang, Z. & Rakich, P. T. RF-Photonic Filters via On-Chip Photonic–Phononic Emit–Receive Operations. *J. Light. Technol.* **36**, 2803–2809 (2018).

100. Choudhary, A. *et al.* On-chip Brillouin purification for frequency comb-based coherent optical communications. *Opt. Lett.* **42**, 5074–5077 (2017).

101. Giacoumidis, E. *et al.* Chip-based Brillouin processing for carrier recovery in self-coherent optical communications. *Optica* **5**, 1191 (2018).

102. Merklein, M. *et al.* Widely tunable, low phase noise microwave source based on a photonic chip. *Opt. Lett.* **41**, 4633–4636 (2016).

103. R. A. Minasian. Photonic signal processing of microwave signals. *IEEE Trans. Microw. Theory Tech.* **54**, 832–846 (2006).

104. Merklein, M., Stiller, B. & Eggleton, B. J. Brillouin-based light storage and delay techniques. *J. Opt.* **20**, 083003 (2018).

105. Liu, Y., Choudhary, A., Marpaung, D. & Eggleton, B. J. Chip-Based Brillouin Processing for Phase Control of RF Signals. *IEEE J. Quantum Electron.* **54**, 6300413 (2018).

106. Wang, Y. *et al.* Improved dual-wavelength-pumped supercontinuum generation in an all-fiber device. in *Optics InfoBase Conference Papers* (2010).

107. Okawachi, Y. *et al.* Tunable All-Optical Delays via Brillouin Slow Light in an Optical Fiber. *Phys. Rev. Lett.* **94**, 153902 (2005).

108. Pant, R. *et al.* Photonic-chip-based tunable slow and fast light via stimulated Brillouin scattering. *Opt. Lett.* **37**, 969–971 (2012).

109. Mckay, L. *et al.* Brillouin-based phase shifter in a silicon waveguide. *arXiv.org* **arXiv:1903**,

110. Song, K. Y., Lee, L., & K. & B., S. Tunable optical delays based on Brillouin dynamic grating in optical fibers. *Opt. Express* **17**, 10344–10349 (2009).

111. Marco Santagiustina, S. C., Primerov, N., & L. U. & Thévenaz, L. All-optical signal processing using dynamic Brillouin gratings. *Sci. Rep.* **3**, 1594 (2013).

112. Preußler, S. *et al.* Quasi-Light-Storage based on time-frequency coherence. *Opt. Express* **17**, 15790–15798 (2009).

113. Zhu, Z., Gauthier, D. J. & Boyd, R. W. Stored Light in an Optical Fiber via Stimulated Brillouin Scattering. *Science (80-.).* **318**, 1748–1753 (2007).

114. Merklein, M., Stiller, B., Vu, K., Madden, S. J. & Eggleton, B. J. A chip-integrated coherent photonic-phononic memory. 8, 574 (2017). *Nat. Commun.* **8**, 574 (2017).

115. Merklein, M., Stiller, B. & Eggleton, B. J. Brillouin-based light storage and delay techniques. *J. Opt.* **20**, 083003 (2018).

116. Lenz, G., Eggleton, B. J., Madsen, C. K. & Slusher, R. E. Optical delay lines based on optical filters. *IEEE J. Quantum Electron.* **37**, 525–532 (2001).

117. Aryanfar, I. *et al.* Chip-based Brillouin radio frequency photonic phase shifter and wideband time delay. *Opt. Lett.* **42**, 1313–1316 (2017).

118. Jalas, D. *et al.* What is — and what is not — an optical isolator. *Nat. Photonics* **7**, 579–583 (2013).

119. Fang, K., Yu, Z. & Fan, S. Realizing effective magnetic field for photons by controlling the phase of dynamic modulation. *Nat. Photonics* **6**, 782–787 (2012).

120. Kang, M. S., Butsch, A. & Russell, P. S. J. Reconfigurable light-driven opto-acoustic isolators in photonic crystal fibre. *Nat. Photonics* **5**, 549–553 (2011).

121. Kuhn, L., Heidrich, P. F. & Lean, E. G. Optical guided wave mode conversion by an acoustic surface wave. *Appl. Phys. Lett.* **19**, 428–430 (1971).

122. Hwang, I. K., Yun, S. H. & Kim, B. Y. All-fiber-optic nonreciprocal modulator. *Opt. Lett.* **22**, 507 (1997).

123. Huang, X. & Fan, S. Complete all-optical silica fiber isolator via stimulated Brillouin scattering. *J. Light. Technol.* **29**, 2267–2275 (2011).

124. Poulton, C. G. *et al.* Design for broadband on-chip isolator using Stimulated Brillouin Scattering in dispersion-engineered chalcogenide waveguides. *Opt. Express* **20**, 21235–46 (2012).

125. Kittlaus, E. A., Otterstrom, N. T., Kharel, P., Gertler, S. & Rakich, P. T. Non-reciprocal interband Brillouin modulation. *Nat. Photonics* **12**, 613–619 (2018).

126. Sohn, D. B., Kim, S. & Bahl, G. Breaking time-reversal symmetry with acoustic pumping of nanophotonic circuits. *Nat. Photonics* **12**, 91–98 (2018).

127. Kim, J., Kim, S. & Bahl, G. Complete linear optical isolation at the microscale with ultralow loss. *Sci. Rep.* **7**, 1647 (2017).

128. Bao, X., D. J. Webb, A. & Jackson, D. A. 32-km distributed temperature sensor based on Brillouin loss in an optical fiber,. *Opt. Lett.* **18**, 1561–1563 (1993).

129. Nikles, M., Luc Thévenaz, A. & Robert., P. A. Simple distributed fiber sensor based on Brillouin gain spectrum analysis. *Opt. Lett.* **21**, 758–760 (1996).

130. Minardo, A., Bernini, R., Amato, L. & L. Zeni. Bridge monitoring using brillouin fiber-optic sensors. *IEEE Sens. J.* **12**, 145–150 (2011).

131. Kurashima, T., T. Horiguchi, A. & M. Tateda. Distributed-temperature sensing using stimulated Brillouin scattering in optical silica fibers. *Opt. Lett.* **15**, 1038 (1990).

132. Thévenaz, L. Brillouin distributed time-domain sensing in optical fibers: state of the art and perspectives. *Front. Optoelectron. China* **3**, 13–21 (2010).

133. Hotate, K., & Hasegawa, T. Measurement of Brillouin Gain Spectrum Distribution along an Optical Fiber Using a Correlation-Based Technique--Proposal, Experiment and Simulation. *IEICE Trans. Electron.* **83**, 405–412 (2000).

134. Fellay, A., Thévenaz, L., Facchini, M., Niklès, M. & Robert, P. Distributed sensing using stimulated Brillouin scattering : towards ultimate resolution. in *in 12th International Conference on Optical Fiber Sensors* OWD3 (1997).

135. Hotate, K., Watanabe, R., He, Z. & Kishi, M. Measurement of Brillouin frequency shift distribution in PLC by Brillouin optical correlation domain analysis. in *in 12th International Conference on Optical Fiber Sensors* 8421 (International Society for Optics and Photonics, 2012).

136. Zarifi, A. *et al.* Highly localized distributed Brillouin scattering response in a photonic integrated circuit. *APL Photonics* **3**, 036101 (2018).

137. Zarifi, A. *et al.* Brillouin spectroscopy of a hybrid silicon-chalcogenide waveguide with geometrical variations. *Opt. Lett.* **43**, 3493–3496 (2018).

138. Zarifi, A. *et al.* On-chip correlation-based Brillouin sensing: design, experiment, and simulation. *J. Opt. Soc. Am. B* **36**, 146–152 (2019).

139. Chow, D. M., Yang, Z., Soto, M. A. & Thévenaz, L. Distributed forward Brillouin sensor based on local light phase recovery. *Nat. Commun.* **9**, 2990 (2018).

140. Bashan, G., Diamandi, H. H., London, Y., Preter, E. & Zadok, A. Optomechanical time-domain reflectometry. *Nat. Commun.* **9**, 2991 (2018).

141. East, P. W. Fifty years of instantaneous frequency measurement. *IET Radar, Sonar Navig.* **6**, 112–122 (2012).

142. Jiang, H. *et al.* Wide-range, high-precision multiple microwave frequency measurement using a chip-based photonic Brillouin filter. *Optica* **3**, 30–34 (2016).

143. Scheuer, J. Fiber microcoil optical gyroscope. *Opt. Lett.* **34**, 1630–1632 (2009).

144. Ferreira, M. F., J. F. Rocha, A. & Pinto, J. L. Analysis of the gain and noise characteristics of fiber Brillouin amplifiers. *Opt. Quantum Electron.* **26**, 35–44 (1994).

145. Feng, C., S. Preussler & Schneider, T. Sharp tunable and additional noise-free optical filter based on Brillouin losses. *Photon. Res.* **6**, 132 (2018).

146. Mahendra, A. *et al.* High link performance of Brillouin-loss based microwave bandpass photonic filters. *OSA Contin.* **1**, 1287–1297 (2018).

147. Wei, W., Yi, L., Jaouën, Y., Morvan, M. & Hu, W. Brillouin Rectangular Optical Filter With Improved Selectivity and Noise Performance. *IEEE Photonics Technol. Lett.* **27**, 1593–1596

(2015).

148. Leonardo Midolo, A. S. & A. F. Nano-opto-electro-mechanical systems. *Nat. Nanotechnol.* **13**, 11–18 (2018).

149. Rakich, P. T., Wang, Z. & Davids, P. Scaling of optical forces in dielectric waveguides: rigorous connection between radiation pressure and dispersion. *Opt. Lett.* **36**, 217 (2011).

150. Laude, V. & Beugnot, J. C. Lagrangian description of Brillouin scattering and electrostriction in nanoscale optical waveguides. *New J. Phys.* **17**, 0–13 (2015).

151. Sipe, J. E. & Steel, M. J. A Hamiltonian treatment of Stimulated Brillouin Scattering in nonlinear integrated waveguides. *New J. Phys.* **18**, 045004:1–21 (2016).

152. Kharel, P., Behunin, R. O., Renninger, W. H. & Rakich, P. T. Noise and dynamics in forward Brillouin interactions. *Phys. Rev. A* **93**, 063806:1–12 (2016).

153. Van Laer, R., Kuyken, B., Baets, R. & Van Thourhout, D. Unifying Brillouin scattering and cavity optomechanics. (2015).

154. NUMBAT: NUMerical Brillouin Analysis Tool. *http://bit.ly/2lhpA5Y* Available at: http://science.mq.edu.au/~msteel/research/numbat.html. (Accessed: 15th February 2017)

155. Malinowski, M. & Fathpour, S. Fully-Tensorial Elastic-Wave Mode-Solver in FEniCS for Stimulated Brillouin Scattering Modeling. **arXiv:1812**, 1–7 (2018).

156. Kashkanova, A. D. *et al.* Superfluid Brillouin optomechanics. *Nat. Phys.* **13**, 74–79 (2017).

157. Chen, Y.-C., And, S. K. & Bahl, G. Brillouin cooling in a linear waveguide. *New J. Phys.* **18**, 115004 (2016).

158. Zhu, L. & Fan, S. Near-complete violation of detailed balance in thermal radiation. *Phys. Rev. B* **90**, 1–5 (2014).

159. Ma, J. *et al.* On-chip optical isolator and nonreciprocal parity-time symmetry induced by stimulated Brillouin scattering. *arXiv:1806.03169*

160. Kim, S., Taylor, J. M. & Bahl, G. Dynamic suppression of Rayleigh light scattering in dielectric resonators. *arXiv:1803.02366*

161. J. A. Haigh, A. Nunnenkamp, A. J. Ramsay, and A. J. F. Triple-Resonant Brillouin Light Scattering in Magneto-Optical Cavities 117, 133602. *Phys. Rev. Lett.* **117**, 133602 (2016).

162. Smith, M. J. A. *et al.* Metamaterial control of stimulated Brillouin scattering. *Opt. Lett.* **41**, 2338 (2016).

163. Laer, R. Van, Bazin, A., Kuyken, B., Baets, R. & Thourhout, D. Van. Net on-chip Brillouin gain based on suspended silicon nanowires. *New J. Phys.* **17**, 115005 (2015).

164. Madden, S. J. *et al.* Long, low loss etched As2S3 chalcogenide waveguides for all-optical signal regeneration. *Opt. Express* **15**, 14414 (2007).

Material	Intrinsic loss	(p_{11}, p_{12})	n	v_a (m/s)	ρ (kg/m^3)	g_B^{FSBS} (1/W m)	g_B^{BSBS} (1/Wm)
As_2S_3	<0.01 dB/cm	(+0.24, +0.25)	2.4	5915	3430	8.4E-10	3.8E-09
Silica	<1.4E-5 dB/cm	(+0.12, +0.27)	1.5	2527	2203	2.4E-12	5.9E-11
Silicon	<0.01 dB/cm	(-0.09, +0.017)	3.5	8909	2330	1.0E-10	1.8E-11
Ge	<3 dB/cm	(-0.151,-0.128)	2.0	5235	5350	4.6E-09	1.3E-09

Table AA: Table of intrinsic Brillouin parameters for various platforms, together with the resulting Brillouin gain in forward (g_B^{FSBS}) and backwards (g_B^{BSBS}) configurations.

Ref	Year	Material	Scattering Process	Length (cm)	Loss (dB/cm)	Brillouin Frequency (GHz)	Q-factor	Gain G_B (/m/W)	P_p (W)	On-off Gain (dB)	Transmission Loss (dB)	Net Gain (dB)
17	2010	Silica SMF	BSBS	1000000	0	10.9	545	1.82	0.5	50	0	50
24	2011	As_2S_3	BSBS	7	0.4	7.7	226	310.86957	0.3	18.8	2.8	16
108	2012	As_2S_3	BSBS	7	0.4	7.7	214	317.3913	0.3	25.8	2.8	23
39	2017	As_2S_3	BSBS	22	0.5	7.6	760	500	0.5	52	12	40
80	2017	Hybrid As_2S_3	BSBS	5.8	0.7	7.6	181	750	0.5	22.5	4	18.5
25	2013	Silicon	FSBS	0.33	7	1.8-16.3	1000-1800	2750	0.02	0.374264979	2.31	-1.93574
26	2015	Silicon	FSBS	4	0.175	9.2	306	3218	0.025	4.4	4.5	-0.1
163	2015	Silicon	FSBS	2.535	5.5	9.1	728	6561	0.035	2	1.5	0.5
51	2016	Silicon	FSBS	2.9	0.18	4.35	680	1152	0.062	6.9	1.7	5.2
53	2017	Silicon	SIMS	2.3	0.24	6	300	470	0.088	3.5	1.2	2.3
56	2019	Silicon	SIMS (Resonant)			6	300		0.015	30	10	20
33	2019	Dilute Nitride	BSBS	500	0.04	10.93	71	0.1	0.61	1.2	2	-0.8

Table BB: Table of integrated Brillouin measurements and parameters including gain and loss in waveguides compared to SMF (top row).

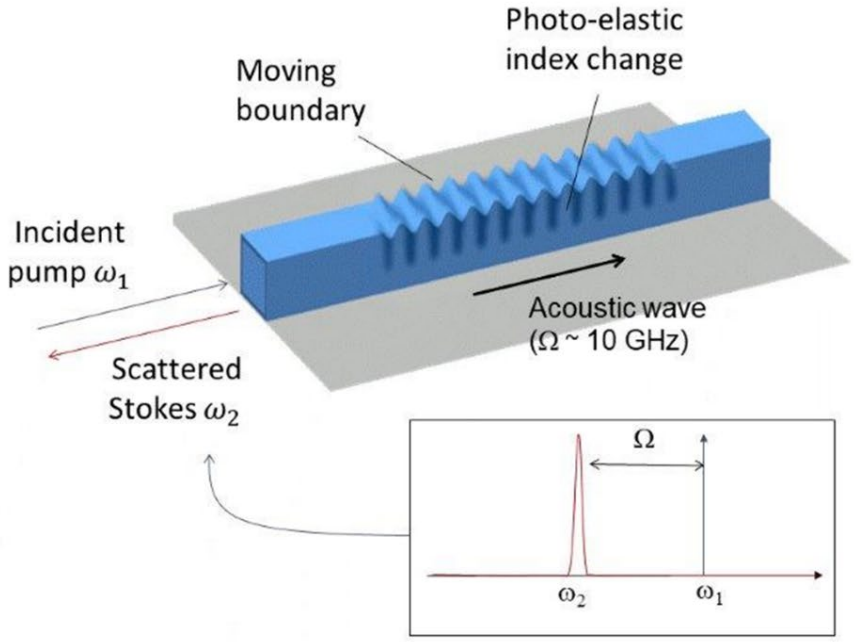

Fig. 1 Overview of Stimulated Brillouin Scattering: A pump wave (ω_1) scatters from and re-enforces an acoustic phonon (Ω) and is downshifted to a Stokes waves (ω_2). The result is a narrow Stokes peak separated at a distance of GHz from the pump. This configuration shows backward Brillouin scattering, however other configurations are possible (see Box 1).

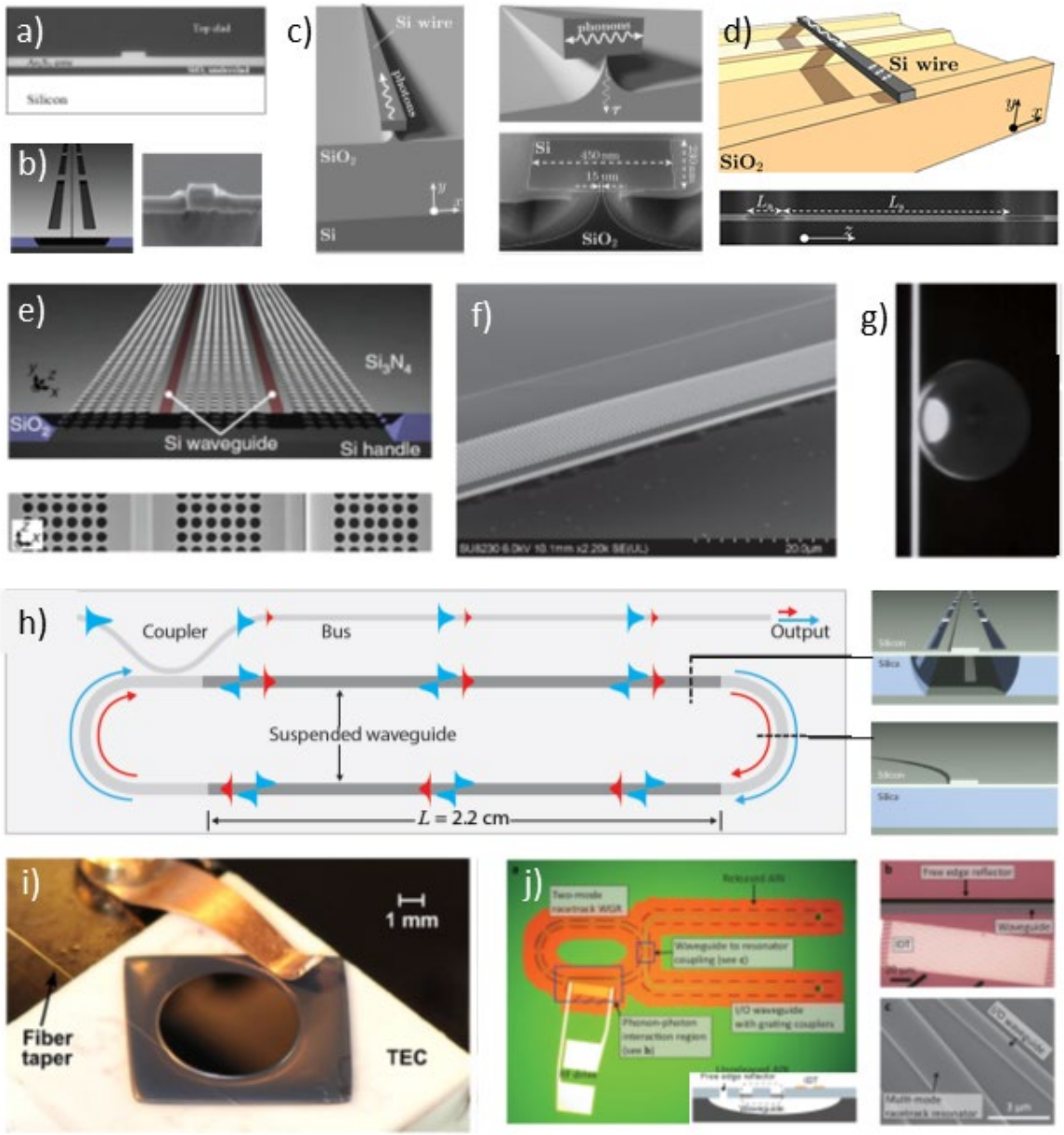

Fig. 2: Different geometries used in on-chip SBS experiments: (a) Chalcogenide (As_2S_3) rib waveguide on silica[164]*; (b) silicon waveguide in silicon nitride*[25]*; (c) Silicon pedestal with silica support*[26]*; (d) Suspended silicon waveguide*[163]*; (e) Dual silicon waveguides with phononic crystal connector*[52]*; (f) Silicon nitride photonic/phononic crystal edge waveguide* [59]*; (g) Silica microresonator*[71]*; (h) Suspended silicon racetrack resonator*[83]*; (i) high-Q silica microresonator*[82]*; (j) Aluminum nitride racetrack resonator used with acoustic modulation* [126]*.*

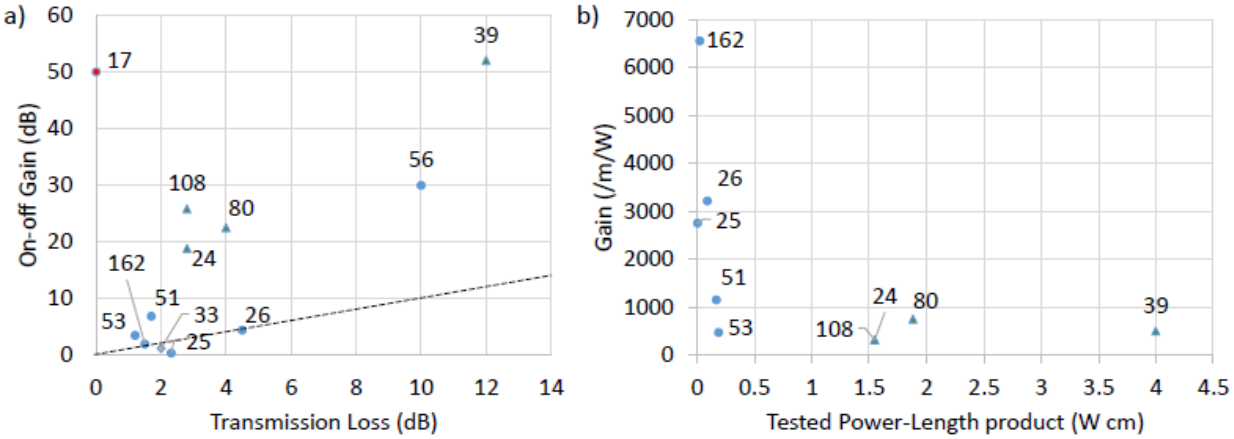

Fig. 3X: a) Measured gain vs loss in Brillouin active waveguides; net gain occurs above the dashed line. b) Waveguide gain (in 1/m/W) in current Brillouin experiments, as plotted against the product between tested power and effective length. Soft glasses have relatively low gains but have larger P_p L_{eff} products, which can be used to generate higher absolute gains, whereas silicon platforms have extremely high intrinsic gains but are deployed with lower powers. Low gain, long length structures such as fibre and dilute silicon nitride[33] are not shown in (b).

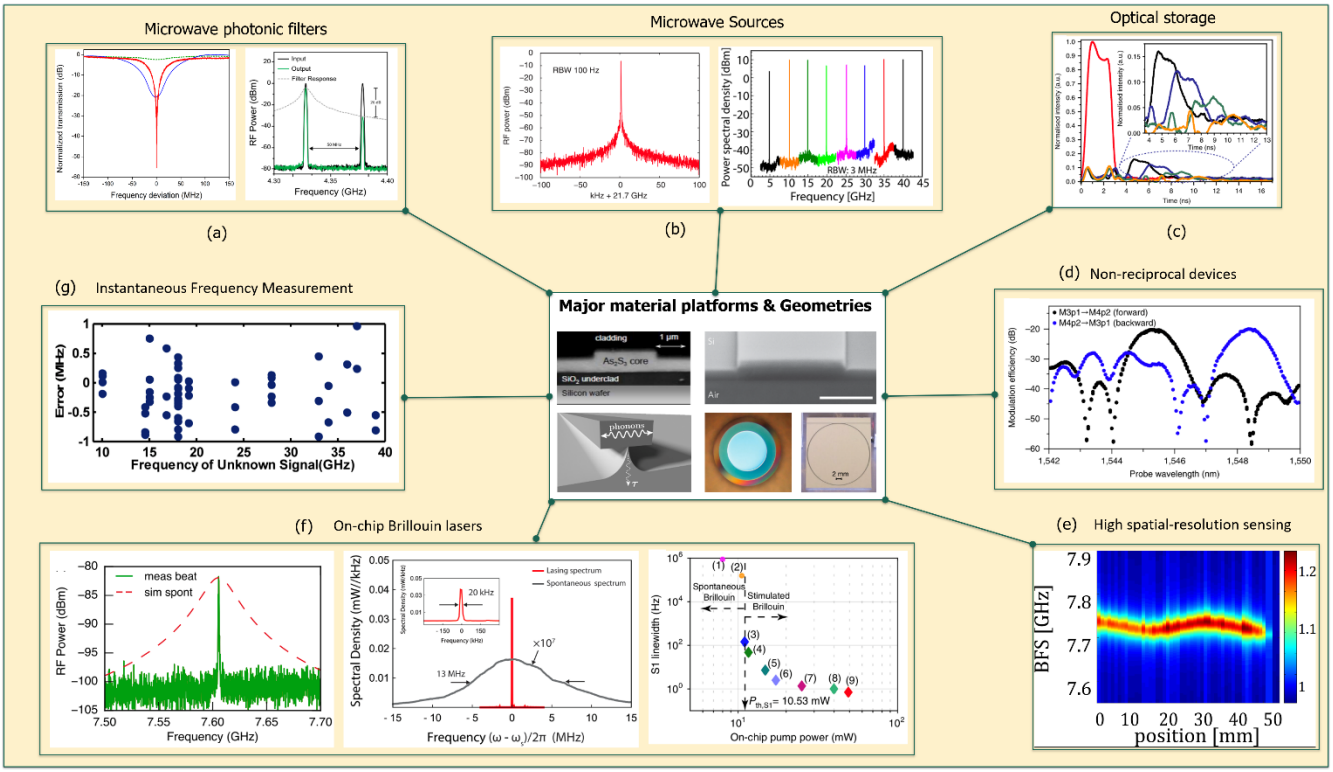

Fig. 4: Functionalities enabled by on-chip SBS. (a) microwave photonic filters [97]*; (b) microwave sources* [102]*; (c) Optical storage* [114]*; (d) non-reciprocal devices* [125]*; (e) high-resolution sensing* [136]*; (f) Brillouin lasers* [33,80,83]*; and (g) instantaneous frequency measurement (IFM)* [142]*.*

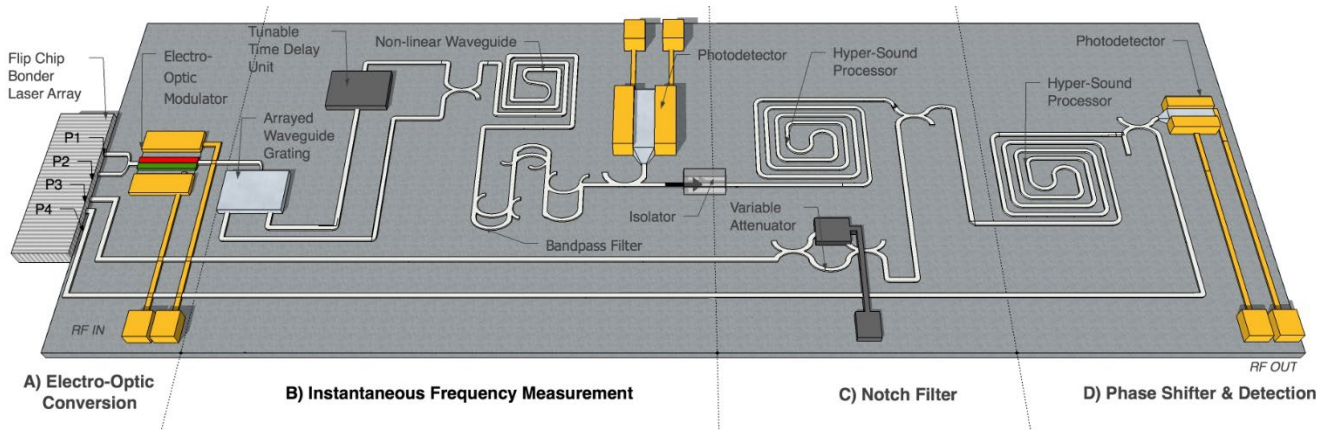

Fig. 5: A chip-scale integrated microwave/RF processor for broadband communications. Incoming RF signals are A) converted to photons and B) spectrally analysed. The desired signal is C) extracted and D) processed before conversion back to RF. Functions B), C) and D) all require strong on-chip opto-acoustic interactions.